Tidal mixing hotspots governed by rapid parametric subharmonic instability

J.A. MACKINNON AND K.B. WINTERS
Scripps Institution of Oceanography, La Jolla, CA

(Manuscript received soon! , in final form soon!)

ABSTRACT

Numerical process studies of an idealized upward propagating internal tide at 21°S demonstrate a rapid transfer of energy (over only a few days) to waves of half the tidal frequency and smaller vertical scale. The energy transfer characteristics are consistent with Parametric Subharmonic Instability (PSI), a particular class of resonant wave-wave interactions previously thought too slow (timescales of weeks or months) to be an effective mechanism for extracting energy from the internal tide. Near sources, the internal tide is coherent, i.e. not well described by a random phase approximation. Consequently, the simulated transfer rates are much faster than theoretical predictions that rely on this approximation. The slow group velocities of recipient subharmonic waves constrain them to break near the generation site; overall 40 % of the tidal energy is dissipated locally. Further simulations indicate that the strength of this "tidal mixing hotspot" is strongly latitude dependent. At the critical latitude of 28.9°nearly 80 % of tidal energy is dissipated locally. Poleward of the critical latitude, $M_2/2 < f$, PSI can not occur, and nearly all the generated tidal energy radiates away.

1. Introduction

Breaking internal waves are the dominant source of deep-ocean mixing. *Munk and Wunsch* (1998) calculate that maintenance of deep stratification requires that on average 2.1 TW of power be drawn from external sources, converted to internal gravity waves and irreversibly transformed to potential energy via small-scale turbulent mixing events. Approximately half (0.9 TW) of the required global internal-wave power is produced by the interaction of the barotropic tide with topography, generating internal-waves of tidal frequency, otherwise known as an internal tide. (The other significant source of internal-wave energy is surface wind stress (*Alford* 2001), though the focus here is on the tide.)

Neither the sources nor turbulent sinks of internal-wave energy are uniformly distributed throughout world oceans. *St. Laurent and Nash* (2004) estimate that 30-50% of energy input into the internal tide is lost to turbulence near the generation site. The result is the increasingly familiar picture of hotspots of elevated mixing near rough topography (*Polzin et al.* 1997; *St. Laurent et al.* 2002; *St. Laurent and Garrett* 2002), a spatially variable process with significant consequences for the global circulation (*Simmons et al.* 2004; *Hasumi and Suginohara* 1999).

While internal waves are primarily generated at medium-large scales (vertical wavelengths of hundreds to thousands of meters), the transition to turbulence is regulated by the highly nonlinear dynamics (e.g. 'breaking') of small-scale waves (vertical wavelengths of tens of meters).The magnitude and spatial extent of turbulent hotspots is controlled by the dynamic or kinematic processes that transfer energy from large- to small-scale motions. Away from the immediate vicinity of boundaries, nonlinear interaction between groups of propagating internal waves (*Müller et al.* 1986; *Henyey et al.* 1986; *Sun and Kunze* 1998) is thought to produce the necessary scale transformations.

We will show here that the internal tide is particularly susceptible to an interaction known as Parametric Subharmonic Instability (PSI); it involves energy transfer from a primary wave of relatively large scale to two 'recipient' waves of smaller vertical scale and approximately half the primary frequency. For the internal tide, energy can be drained through PSI only when the half-frequency recipient waves are within the internal wave band ($M_2/2 \geq f$), a criterion only satisfied equatorward of 28.9°.

Previous work has argued that wave-wave interactions are an inefficient means to transfer of energy out of the internal tide. For example, *Olbers and Pomphrey* (1981) argue that the characteristic timescales for energy transfer through PSI are so slow (weeks to months) as to 'disqualify' PSI as an important mediator of internal wave evolution and associated patterns of turbulence. However, recent observations [*Polzin et al.* (1997) and Rainville, in prep] and numerical studies (*Hibiya et al.* 2002) suggest this disqualification may have been premature. In particular, the theoretical calculations were based on an assumption that the waves in question are in a statistical

Corresponding author address: J.A. MacKinnon, 9500 Gilman Dr., Mail Code 0209, La Jolla, CA
E-mail: jmackinnon@ucsd.edu

steady state with randomly distributed phase and direction, an assumption which may not be appropriate near internal-tide generation sites.

We present results from a series of idealized numerical experiments undertaken to study nonlinear internal wave evolution above sites of topographic internal tide generation. The principal results of this study are that, in the near field of tidal conversion sites, PSI acts on time scales far shorter than previously thought (days), and that the efficient transfer to lower frequency, smaller vertical scale waves controls the vertical distribution of the tidal 'mixing hotspot'.

Numerical methods are described in Section 2. In Section 3 we compare results from three experiments: at, poleward, and equatorward of the critical latitude of 28.9°. Transfer rates in and out of the internal tide are quantified. The effect of the transfers on vertical propagation and the magnitude and vertical scale of elevated mixing regions are discussed in Section 4. Conclusions and implications for global circulation are presented in Section 5.

**** ADDD ***** Toshi and company showed...what? PSI is a fast (less than 10 inertial periods) method of transfering energy out of the tides when there is a spike of energy (CHECK olbers to make sure he's not using a spike too). PSI loosely here, cuz energy in Toshi's simulations goes to a broad band of frequencies. And that it has an on/off latitude dependence. He argues that you should expect nearfield hotspots equatorward of 30, but not poleward. So what do we add to that? One, study rates of energy loss as a function of various parameters and vertical extent of mixing hotspots and relationship between then. Two, look carefully at dynamics of instability. What sets the transfer rate? And it's dependence on latitutde and other things?

2. Numerical Methods

The numerical model used here is an updated version of the three-dimensional, pseudo-spectral nonhydrostatic code used by *Winters and D'Asaro* (1997), and is more fully described in *Winters et al.* (2004). The model solves the equations of motion in an incompressible, rotating ocean with arbitrary forcing,

$$\begin{aligned}
\frac{\partial u}{\partial \mathrm{t}} &= -\vec{u}\cdot\nabla u + fv - \frac{1}{\rho_0}\frac{\partial p'}{\partial \mathrm{x}} + \nu_{\mathbf{p}}\cdot\nabla^p u + F_u \\
\frac{\partial v}{\partial \mathrm{t}} &= -\vec{u}\cdot\nabla v - fu - \frac{1}{\rho_0}\frac{\partial p'}{\partial \mathrm{y}} + \nu_{\mathbf{p}}\cdot\nabla^p v + F_v \\
\frac{\partial w}{\partial \mathrm{t}} &= -\vec{u}\cdot\nabla w - \frac{1}{\rho_0}\frac{\partial p'}{\partial \mathrm{z}} - \frac{g\rho'}{\rho_0} + \nu_{\mathbf{p}}\cdot\nabla^p w + F_w \\
\frac{\partial \rho'}{\partial \mathrm{t}} &= -\vec{u}\cdot\nabla\rho' - w\frac{\partial\overline{\rho}}{\partial \mathrm{z}} + \kappa_{\mathbf{p}}\cdot\nabla^p\rho' + \kappa\frac{\partial^2\overline{\rho}}{\partial \mathrm{z}^2} + F_{\rho'} \\
\nabla\cdot\vec{u} &= 0, \qquad (1)
\end{aligned}$$

where $[u,v,w]$ is the velocity vector, ρ' is the density perturbation from a linearly increasing average density profile, $\overline{\rho}(z)$, p' is the perturbation pressure, ρ_0 is a reference density, and f is the local inertial frequency. The model is solved in a rectangular domain of size (L_x, L_y, L_z) with (n_x, n_y, n_z) evenly spaced grid points, horizontally periodic boundary conditions and free-slip top and bottom boundary conditions (Table 1).

The coefficients $(\nu_{\mathbf{p}}, \kappa_p)$ and exponent $(p = 10)$ of the hyperviscosity terms in (1) are chosen to maximize the range of inviscid wavenumbers while removing energy from the smallest resolved scales quickly enough to maintain numerical stability. In practice, energy is drained from vertical scales smaller than 150 m on timescales shorter than one day. Based upon these equations we define a 'hyperdissipation' rate (henceforth simply referred to as the dissipation rate),

$$\varepsilon_p = \nu_{p,j}\left[\frac{\partial}{\partial x_j}^{p/2} u_{kk}\right]^2 \qquad (2)$$

that describes the rate at which energy is removed from the smallest resolved scales. In steady state, this is equivalent to the rate at which energy is transfered to dissipative scales by the inviscid dynamics at resolved ($\lambda_z \geq 150$ m) scales. An implicit assumption in this approach is that energy does not "pile up" at scales smaller than about 150 m. This assumption is both necessary and reasonable.

Guided by the expected strong latitudinal dependence of PSI, we conducted three otherwise identical experiments at 21° S (Case **A**), 28.9 ° S (Case **B**), and 40 ° S (Case **C**). The simulations are initialized at rest and forced with a monochromatic, bottom-localized field of upward-propagating internal waves of tidal (M_2) frequency. The forcing scheme is a modification of that used by *Slinn and Riley* [1998]. For example, forcing of vertical velocity is specified as the time derivative of a hypothesized forcing wave velocity,

$$\begin{aligned}
F_w &= \frac{\partial w_F}{\partial \mathrm{t}} = -A_0\,\omega_0^2\, e^{i[\mathbf{k_0}\cdot\mathbf{x}-\omega_0 t]}F(z) \qquad (3)\\
\mathbf{k_0} &= [k_{x0}, k_{y0}, k_{z0}(k_x, k_y, \omega_0)] \qquad (4)\\
F(z) &= e^{-b^2 z^2}, \qquad (5)
\end{aligned}$$

where ω_0 is the M_2 tidal frequency, and A_0 the vertical displacement (Table 1). The amplitude was chosen to produce upward tidal energy fluxes of several mW/m, consistent with the results of *St. Laurent and Garrett* (2002). The central horizontal wavevector $[k_{x0}, k_{y0}]$ was chosen to match that of the strongest upward tidal energy fluxes observed in the Brazil Basin (*St. Laurent and Garrett* 2002), and is oriented eastward in these f-plane simulations without loss of generality. The vertical wavenumber is calculated from the dispersion relationship, which depends on latitude; hence k_z varies slightly between the three simulations (Table 1). The characteristic scale, b, of the vertical localization function (F) is chosen to allow at least one full vertical wavelength in the forcing region. Random low-level background noise (rms displacement amplitude of 1 mm) is added through spectrally white forcing at each time step. Waves are not

Table 1. Simulation parameters

Universal Parameters							
$\mathbf{L_x}$	50 km	$\mathbf{n_x}$	128	**N**	2×10^{-3} s^{-1}	$\mathbf{2\pi/k_{x0}}$	10 km
$\mathbf{L_y}$	50 km	$\mathbf{n_y}$	64	$\boldsymbol{\omega_0}$	1.4×10^{-4} s^{-1}	$\mathbf{2\pi/k_{y0}}$	0 km
$\mathbf{L_z}$	5 km	$\mathbf{n_z}$	128	$\mathbf{A_0}$	1.0 m		
Specific Parameters							
Case A	Latitude	21 °S		**f**	-5.3×10^{-5} s^{-1}	$\mathbf{2\pi/k_{z0}}$	654 m
Case B	Latitude	28.9 °S		**f**	-7.0×10^{-5} s^{-1}	$\mathbf{2\pi/k_{z0}}$	611 m
Case C	Latitude	40 °S		**f**	-9.3×10^{-5} s^{-1}	$\mathbf{2\pi/k_{z0}}$	527 m

allowed to reflect off the upper surface, but rather are absorbed by strong Rayleigh friction in a sponge layer in the top few hundred meters.

3. Results

The goal of the idealized simulations presented here is not to replicate a specific oceanic observation, but rather to examine an idealized flow in a similar parameter regime in hopes of extracting dynamical insights and parameter dependencies applicable to oceanic internal tides. Towards that end, our analysis is guided by several motivating questions:

1. How much of the forced internal tidal energy is lost to dissipation in the 'nearfield' of the wave generation site (in our case everywhere below the surface sponge layer)? *St.Laurent and Nash* (2003) suggest on average 30 % , but the variability is not well quantified from limited observations.

2. What are the primary dynamical processes that act to transfer energy to the smaller scales at which it is dissipated? In particular, is PSI important?

3. What role does latitude play in the answer to either question? Are there substantial differences in wave dynamics and dissipation rate patterns equatorward and poleward of the critical latitude cutoff for PSI?

Our approach is twofold. First, we examine the flow as it spins up from rest. Though the flow is unrealistically "clean" in the spinup phase, the wave energy transfers are easy to diagnose and are useful to guide the analysis of the more realistically complex flows that subsequently evolve. Second, we look at wave distribution and energetics once the simulation has reached steady-state.

Case A: 21 ° S - equatorward of the critical latitude

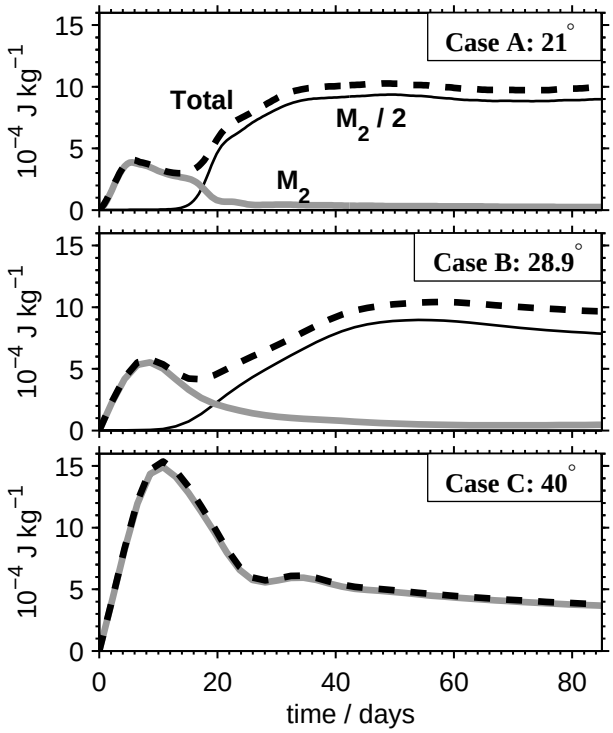

FIG. 2. Top: evolution of total energy (dotted) and spectrally integrated energy in the M_2 (thick,grey) and $M_2/2$ (thin, black) frequency bands for Case A (21 °). Middle, Bottom: same for Cases B and C. Frequency spectra at each time were calculated from wavenumber spectra and the linear dispersion relationship.

For the first few days the dominant feature is a monochromatic coherent upward propagating tide, the angle of which is consistent with the M_2 tidal frequency (Fig. 1, upper left). Spectral energy density is concen-

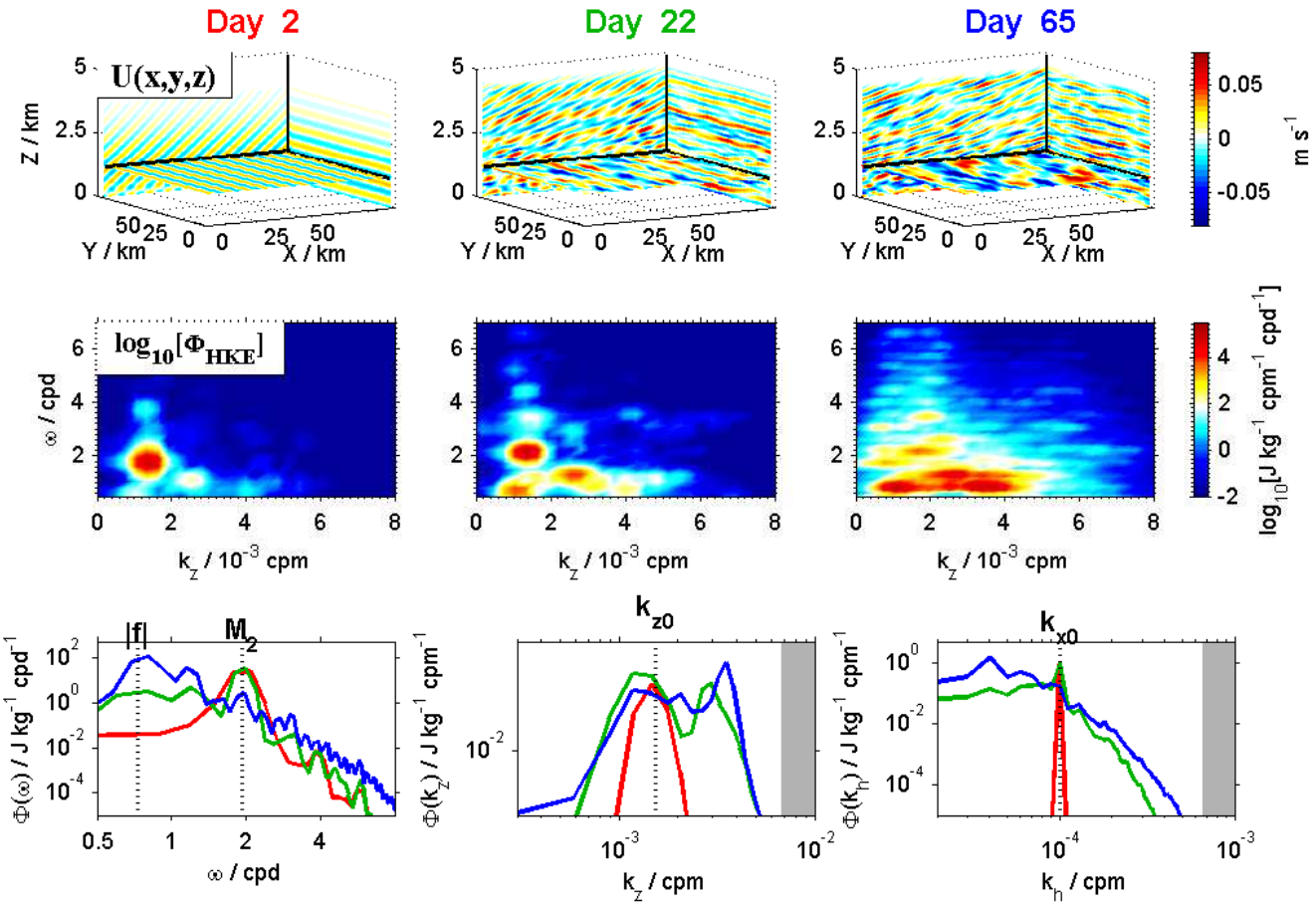

FIG. 1. Snapshots at three times during the evolution of an upward propagating internal tide at 21 ° S (case A, Table 1). Top row: eastward horizontal velocity. Middle row: spectral (horizontal kinetic) energy density as a function of vertical wavenumber and frequency, calculated from 4 day time series surrounding the times of each snapshot in the top row. Bottom row: power spectra for each time period as a function of (from left to right) frequency, vertical wavenumber, and horizontal wavenumber: day 2(red), day 22(green), and day 65(blue).

trated near the forcing frequency and wavenumber (Fig. 1, middle left panel and red lines in bottom three panels). Energy in this frequency band initially grows quickly (Fig. 2), as generated waves are almost exactly in phase with the forcing. As the waves propagate upwards and away over the second week, the forcing efficiency declines, resulting in a gradual decrease in total tidal energy. During this fortnight there is also a gradual increase in the spectral level of background wave noise (not shown).

Over the third week there is a rapid transfer of energy from tidal (M_2) to subharmonic ($M_2/2$) frequency motions (Fig. 2). Subharmonic waves are visible as an emerging disturbance in horizontal velocity (Fig. 1, upper middle panel), with shallower phase angles indicating lower frequency waves. The energy transfer is more easily seen in a frequency-wavenumber energy spectrum, which reveals the appearance of enhanced energy at two distinct vertical wavenumbers, both near half the original frequency (Fig. 1, middle middle panel).

A closer look at this period shows energy being transfered to two wave packets that, together with the forced internal tide, compose a classic resonant triad (Sec. 4b). Guided by the three discrete peaks in spectral energy density (Fig. 1, middle middle), we bandpass velocity between days 10 and 22 into three frequency bands: near the tidal frequency, just above the subharmonic, and just below the subharmonic (Fig. 3, lower left). Time series of bandpassed velocity (from a representative slice of the spatial domain) show energy transfer from the primary (M_2) wave to two other wave groups – one just above the subharmonic frequency with downward phase propagation (upward energy propagation), and one with just below the subharmonic frequency with upward phase propagation (downward energy propagation), all with well defined characteristic vertical wavenumbers. The frequencies and wavenumbers of these three energy-containing waves add up to form near-perfect triads (Fig. 3, bottom row), as predicted by resonant interaction theory (*Müller et al.* 1986). As time goes on other simple triads emerge in different parts of the spatial domain, all with slightly

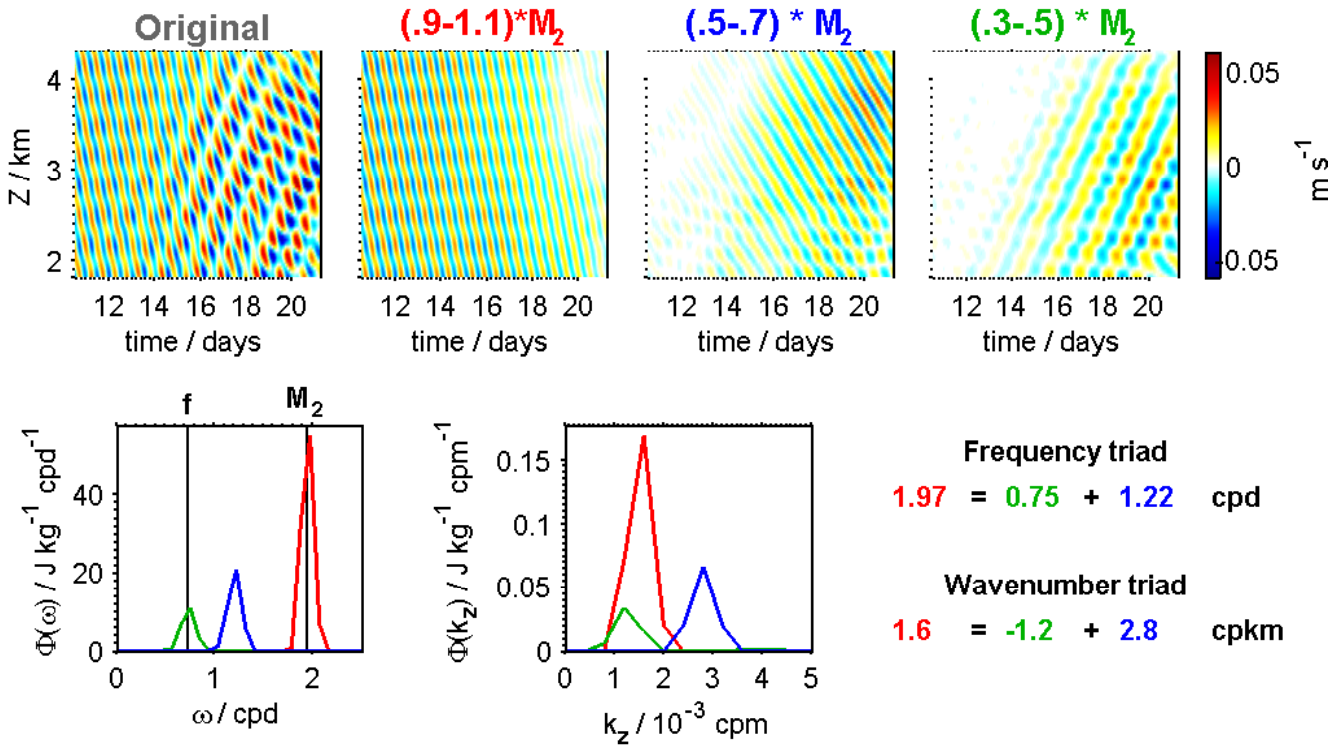

FIG. 3. Top row: time series of (from left to right) eastward horizontal velocity, and horizontal velocity bandpassed in three frequency ranges, as indicated above each plot. Bottom row: one-dimensional frequency and vertical wavenumber spectra of the three bandpassed time series; colors correspond to the titles above each timeseries in the top row. The peak frequencies and vertical wavenumbers of each bandpassed time series are written in the bottom right.

different frequency/wavenumber combinations that add up to locally complete triads (not shown).

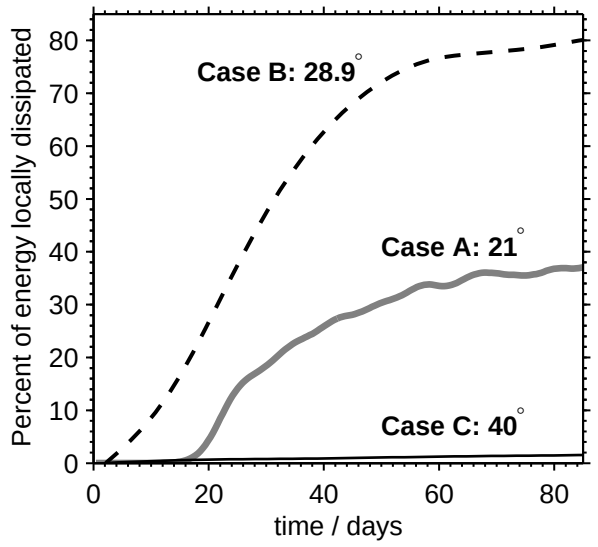

FIG. 4. Percent of energy input through forcing dissipated in the bottom 3800 m (below the surface sponge layer).

After about a month a near steady-state is established, in which the energy level is stabilized and spectral shapes evolve only slowly. In steady-state, energy is input into the internal tide at a rate of 10^{-3} W m^{-2}, 40 % of which is lost to dissipation before waves reach the upper sponge layer (Fig. 4). Depth-averaged spectra show a substantial accumulation of energy near the subharmonic frequency at a range of vertical wavenumbers, primarily at smaller scales (Fig. 5d). Remarkably, though energy is continually being added to tidal frequency waves, spectra show no tidal peak, but rather a red power-law behavior, reminiscent of numerous ocean observations and models (Fig. 1, bottom left).

Depth-averaging masks substantial vertical variations in all steady-state quantities. Both total energy and the rate of energy dissipation smoothly decrease with height above bottom (Fig. 6, left panels, solid black lines). Energy spectra at all depths show peaks at the tidal frequency and two near-subharmonic frequencies, though almost all the energy has accumulated at the lower, near-inertial peak (Fig. 6). The change in relative energy distribution with height can be seen more clearly in spectra of energy flux, which more heavily weight higher-frequency (faster propagating) waves (Fig. 6, upper right panel). Near the bottom, energy flux is primarily tidal, but shifts progressively to subharmonic waves with in-

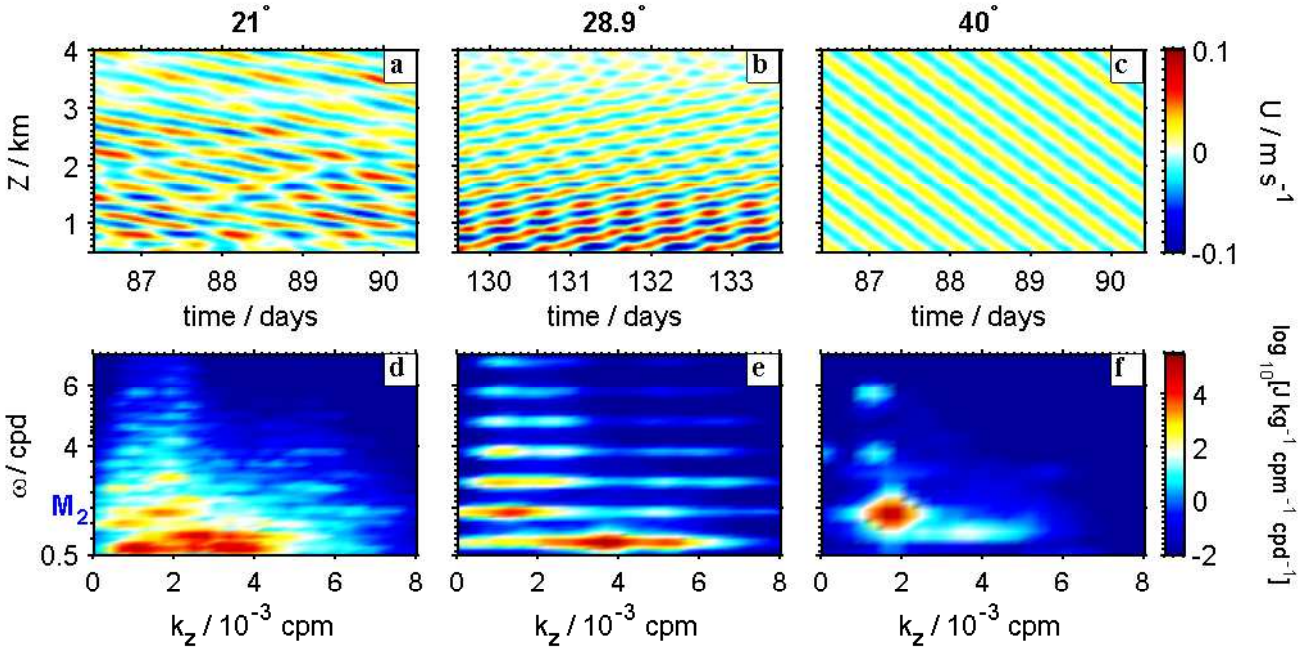

FIG. 5. Top row: select time series of eastward horizontal velocity from each run once a near steady-state has been reached. Bottom row: spectral energy density as a function of frequency and vertical wavenumber for each case.

creasing height. In this sense, the steady-state vertical structure mirrors the evolution in time observed during the spinup period. Summing over all frequencies, the upward energy flux steadily declines with increasing height above the bottom. In steady-state, this flux convergence is balanced by turbulent dissipation.

Case B: 28.9 ° S - at the critical latitude

At the critical latitude (where the subharmonic, $M_2/2$, is equal to the local inertial frequency), energy is rapidly transfered to waves with both subharmonic and harmonic frequencies (Fig. 5e). The largest energy accumulation is at the subharmonic frequency, at slightly higher wavenumbers than in the lower latitude case (Fig. 5, middle middle panel). These near-inertial waves have vanishingly small group velocities and hence negligible upward energy flux (Fig. 6). Rather than propagate upwards and away as in Case A, critical latitude subharmonic waves are bottom-trapped, dissipating near the generation site (Fig. 5b, and grey line in leftmost panel of Fig. 6). For a similar rate of energy input, the near-bottom dissipation rate is triple that at lower latitude (Fig. 6, second from left, compare solid black and grey lines). Nearly all (80 %) of the energy input into the internal tide is dissipated before waves reach the upper sponge layer (Fig. 4 and Fig. 6, leftmost panel).

Case C: 40 ° S - poleward of the critical latitude

In stark contrast to the previous two cases, at 40 °the internal tide does not succumb to any strong instability or wave-wave interaction. Months into the simulation, energy remains tightly concentrated near the forcing frequency and wavenumber (Fig. 5). In steady-state, both energy and energy flux remain at the M_2 tidal frequency at all depths (Fig. 6, bottom row of right two columns). With energy remaining at the relatively large vertical scales at which it is generated, dissipation is negligible (Fig. 6, left), and nearly and virtually all the generated tidal energy propagates unhindered into the upper sponge layer (Fig. 4).

4. Discussion

a. Predicted wave-wave interaction efficiency

Nonlinear energy transfer between internal waves has often been conceptualized with resonant wave-wave interaction theory. In this view, energy is transfered between a triad of weakly nonlinear waves through the first order term of a perturbation expansion in wave amplitude (*McComas* 1977; *Olbers* 1983; *Müller et al.* 1986). The interaction is strongest when participating wavenumbers and frequencies satisfy simple resonance conditions (Fig. 3). Two limiting cases are often considered. The first limit is that of energy transfer between three individually coherent waves. The simplest dimensional scaling of the time rate of change and inertial terms in the moment equation gives a timescale of energy transfer of (*Staquet and Sommeria* 2002)

$$\tau_{\text{simple}} = \frac{L}{U}, \tag{6}$$

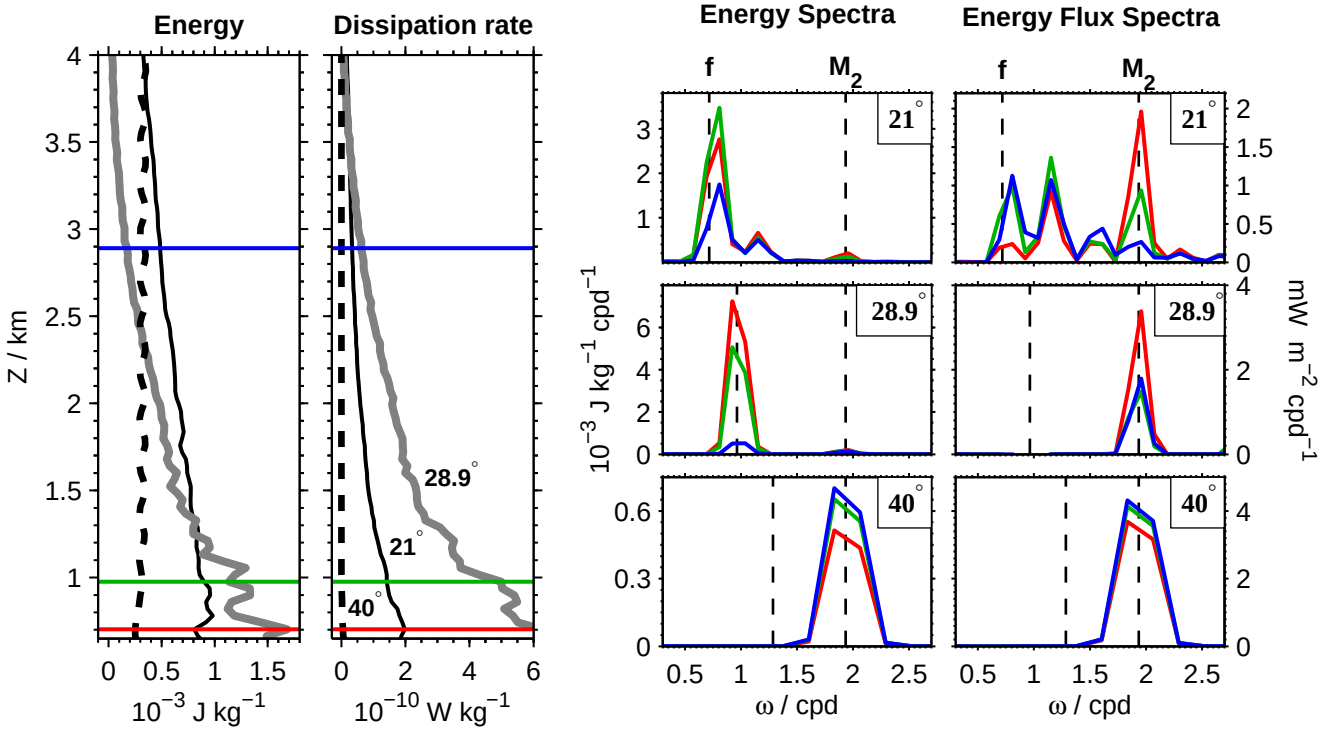

FIG. 6. Left: steady-state average vertical structure of energy (kinetic plus potential) and dissipation rate (2)for simulations at 21 °(solid), 28.9 °(dash-dot), and 40 °(dash). The horizontal colored lines indicate the depths of spectra shown in the right two columns. Second from right column: energy spectra for each latitude (top to bottom) at three representative depths. The M_2 tidal frequency and the local inertial frequency are indicated with vertical dotted lines for reference in each case. Rightmost column: same, for energy flux spectra, calculated as the product of vertical velocity and perturbation pressure using the method of Kunze *Althaus et al*. (2003). Note the change in axis range.

where L is a vertical wavelength and U a rms horizontal velocity. For the internal tide considered here,

$$\tau_{\text{simple}} \approx 2 \text{ days}.$$

On the other hand, most applications of resonant interaction theory to oceanic internal-waves have considered not individually coherent waves but large ensembles of waves with gaussian amplitude and phase distributions. In this statistical limit, ensemble averaging eliminates the first order perturbation term and resonant interactions are controlled by the next perturbative order, resulting in a significantly reduced transfer rate. The random phase approximation provides a good description of wave interactions in the higher-frequency, higher-wavenumber portion of the continuum, as attested to by the successful comparison of resultant mixing parameterizations and turbulence observed in the open ocean thermocline (*Gregg* 1989; *Polzin et al.* 1995). However, the predicted rates of energy transfer out of moderate to low mode internal tides are an order of magnitude lower than observed here. For example, *Olbers and Pomphrey* (1981) suggest that the characteristic timescale for energy transfer out of a mode 10 internal tide is

$$\tau_{OP} \approx 20 \text{ days},$$

and longer for lower modes (their Fig. 1).

The order of magnitude difference in timescale has significant consequences for predicting enhanced mixing near wave-generation sites. An internal tide of the wavelength considered here would propagate upwards to the thermocline or surface in 4-5 days. If the shorter timescale, τ_{simple} is appropriate, the tide should lose a substantial amount of its energy in deep waters, resulting in a mixing hotspot. However, if the more commonly invoked slower timescale, τ_{OP}, is used, the internal tide will escape the generation site to dissipate elsewhere.

b. Observed wave-wave interaction efficiency

The simulations described here demonstrate that PSI can be a rapid means of transferring energy from the internal tide to subharmonic waves of smaller vertical scale at and below 28.9 °. Rapid energy transfers (a few days) are clearly visible during the initial period of wave evolution (Figs. 2, 3). Once a broadband steady-state has been achieved, it is more difficult to observe individual instances of energy transfer. However, the lack of spectral peak at the M_2 frequency (Figs. 1, 6), despite continuous tidal forcing, suggests that the steady state nonlinear energy transfer rate is quick enough to keep up with this applied (and oceanographically realistic) rate of baroclinic

tidal forcing.

A more quantitative estimate of the energy transfer rate can be derived from a consideration of the internal tide energy budget. In steady-state, energy is added to the internal tide at a rate of $10^{-3}\,\mathrm{W\,m^{-2}}$. Tidal energy escapes the nearfield and is absorbed into the upper sponge layer at a rate of $2\times10^{-4}\,\mathrm{W\,m^{-2}}$ (vertical energy flux at the base of sponge layer, Fig. 6). Since the generated tide is of too large a scale to directly dissipate, the remaining $8\times10^{-4}\,\mathrm{W\,m^{-2}}$ must be lost through nonlinear interactions. The characteristic timescale of energy transfer (τ_{model}) can be taken as the ratio of integrated tidal energy and the rate of energy transfer out of the tide,

$$\tau_{\mathrm{model}} \sim \frac{E_{M2}}{[dE/dt]_{\mathrm{nonlin}}} \quad (7)$$

$$= \frac{135\ \mathrm{J\,m^{-2}}}{8\times10^{-4}\ \mathrm{W\,m^{-2}}} \quad (8)$$

$$= 2\ \mathrm{days}. \quad (9)$$

The similarity between the timescale of wave-wave interaction inferred from model results, τ_{model}, and that predicted by simple resonant interaction theory, τ_{simple} suggests that coherent wave-wave interaction theory is more appropriate in the nearfield of wave-generation sites than the random phase statistical limit. The fact that mixing hotspots are actually observed over rough topography (*Polzin et al.* 1997) further supports this conclusion. Other recent studies have also argued that fast energy transfer through PSI plays an important role in the fate of the internal tide (*Hibiya et al.* (2002), and Rainville, in prep.)

c. Latitude dependence of tidal mixing hotspots

The magnitude and spatial distribution of elevated turbulence is controlled by the propensity for efficient wave-wave interaction (PSI) to occur and the group speed of the resultant subharmonic waves. Both factors vary strongly with latitude, leading to order one differences in the magnitude and structure of enhanced dissipation:

- Equatorward of the critical latitude (Case A), PSI provides an efficient transfer of energy from the internal tide to a range of waves with frequencies near the subharmonic ($M_2/2$) and generally smaller vertical scales (Fig. 5). The recipient waves are super-inertial enough to carry substantial upward energy flux (Fig. 6), allowing over half the input energy to propagate away from the 'nearfield' of wave generation (Fig. 4). The result is a moderately strong elevation of turbulence above the generation region, the vertical extent of which is governed by a balance between the group speed and dissipation rate of subharmonic waves.

- At the critical latitude, PSI again quickly transfers energy to subharmonic waves. However in this case the recipient waves are almost exactly inertial (vanishing group velocity) and carry negligible energy flux (Fig. 6). As a result, energy is trapped closer to the generation site, leading to a mixing hotspot three times as strong as at lower latitude.

- Poleward of the critical latitude, no significant wave interactions occur, and nearly all the generated tidal energy propagates away from the generation site. There is no mixing hotspot (Fig. 6).

5. Conclusions

Complementary numerical and theoretical studies demonstrate that the detailed patterns of vertically and laterally inhomogeneous mixing may have striking effects on the structure and magnitude of global circulation patterns. In particular, recent modeling studies (*Simmons et al.* 2004; *Hasumi and Suginohara* 1999) have investigated the effects of a simple enhanced localized mixing over internal tide generation sites. They find that the resulting global and basin-scale flow patterns differ significantly from those calculated with uniform diffusivities.

Effective modeling and prediction of tidal mixing and it's consequences therefore requires two things - a global map of internal tide generation sites, and a dynamical model predicting the fraction of generated baroclinic energy lost to locally enhanced dissipation. The internal-wave generation problem has received a surge of recent attention (*St. Laurent and Nash* 2004; *St. Laurent and Garrett* 2002; *Llewellyn Smith and Young* 2002; *Egbert and Ray* 2000, e.g). Efficient generation is found to occur over a wide range of topography, from fracture zones to sea-mounts to island arcs to mid-ocean ridges. *St. Laurent and Nash* (2004) suggest that on average 30 % of generated energy is lost to produce local mixing hotspots near tidal conversion sites. Our results imply that this percentage has an order one dependence on latitude, ranging from 0% to to 80% over the latitude range considered here. Judicious synthesis of low-mode (energy-containing) internal wave source distributions (both tidal and near-inertial) with latitude dependent predictions of dissipation (from this and future studies) would effectively "close" the internal-wave mixing problem.

Acknowledgements.

This work was sponsored by NSF (OCE 0242471) and ONR (N0014-96-1-0616). We appreciate the insights and perspective shared by Rob Pinkel, Jody Klymak, Kurt Polzin, Peter Muller, and all the HOME investigators.

REFERENCES

Alford, M. H., Internal swell generation: The spatial distribution of energy flux from the wind to mixed layer near-inertial motions, *J. Phys. Oceanogr.*, *31*, 2359–2368, 2001.

Althaus, A., E. Kunze, and T. Sanford, Internal tide radiation from Mendocino Escarpment, *J. Phys. Oceanogr.*, *33*, 1510–1527, 2003.

Egbert, G. D., and R. D. Ray, Significant dissipation of tidal energy in the deep ocean inferred from satellite altimeter data, *Nature*, *405*, 775–778, 2000.

Gregg, M. C., Scaling turbulent dissipation in the thermocline, *J. Geophys. Res.*, *94*, 9686–9698, 1989.

Hasumi, H., and N. Suginohara, Effects of locally enhanced vertical diffusivity over rough bathymetry on the world ocean circulation, *J. Geophys. Res.*, *104*, 23,367–23,374, 1999.

Henyey, F. S., J. Wright, and S. M. Flatté, Energy and action flow through the internal wave field, *J. Geophys. Res.*, *91*, 8487–8495, 1986.

Hibiya, T., M. Nagasawa, and Y. Niwa, Nonlinear energy transfer within the oceanic internal wave spectrum at mid and high latitudes, *J. Geophys. Res.*, *107*, 2002.

Llewellyn Smith, S., and W. R. Young, Conversion of the barotropic tide, *J. Phys. Oceanogr.*, *32*, 1554–1566, 2002.

McComas, C. H., Resonant interaction of oceanic internal waves, *J. Geophys. Res.*, *82*, 1397–1412, 1977.

Müller, P., G. Holloway, F. Henyey, and N. Pomphrey, Nonlinear interactions among internal gravity waves, *Rev. Geophys*, *24*, 493–536, 1986.

Munk, W., and C. Wunsch, Abyssal recipes II: Energetics of tidal and wind mixing, *Deep-Sea Res. Part I*, *45*, 1977–2010, 1998.

Olbers, D., and N. Pomphrey, Disqualifying two candidates for the energy balance of oceanic internal waves, *J. Phys. Oceanogr.*, *11*, 1423–1425, 1981.

Olbers, D. J., Models of the oceanic internal wave field, *Rev. Geophys. Space Physics*, *21*, 1567–1606, 1983.

Polzin, K., J. Toole, J. Ledwell, and R. Schmitt, Spatial variability of turbulent mixing in the abyssal ocean, *Science*, *276*, 93–96, 1997.

Polzin, K. L., J. M. Toole, and R. W. Schmitt, Finescale parameterizations of turbulent dissipation, *J. Phys. Oceanogr.*, *25*, 306–328, 1995.

Simmons, H., S. Jayne, L. S. Laurent, and A. Weaver, Tidally driven mixing in a numerical model of the ocean general circulation, *Ocean Modelling*, *6*, 245–263, 2004.

St. Laurent, L., and C. Garrett, The role of internal tides in mixing the deep ocean, *J. Phys. Oceanogr.*, *32*, 2882–2899, 2002.

St. Laurent, L., and J. Nash, An examination of the radiative and dissipative properties of the internal tides, *Deep-Sea Res.*, *51*, 3029–3042, 2004.

St. Laurent, L., H. Simmons, and S. Jayne, Estimating tidally driven mixing in the deep ocean, *Geophys. Res. Lett.*, *29*, 2002.

Staquet, C., and J. Sommeria, Internal gravity waves: from instabilities to turbulence, *Ann. Rev. Fluid Mech.*, *34*, 559–593, 2002.

St.Laurent, L. C., and J. D. Nash, On the fractino of internal tide energy dissipated near topography, in *Near-Boundary Processes and Their Parameterization*, *Proceedings of the 13th 'Aha Huliko'a Hawaiian Winter Workshop*, edited by P. Muller and D. Henderson, pp. 45–58, 2003.

Sun, H., and E. Kunze, Internal wave/wave interactions: Part I. the role of internal wave vertical diergencevviiical, 1998, submitted to jpo.

Winters, K. B., and E. A. D'Asaro, Direct simulation of internal wave energy transfer, *J. Phys. Oceanogr.*, *27*, 1937–1945, 1997.

Winters, K. B., J. A. MacKinnon, and B. Mills, A spectral model for process studies of rotating, density-stratified flows, *J. Atmos. Ocean. Tech.*, *21*, 69–94, 2004.

Generated with ametsocjmk.cls.

Written by J. M. Klymak

mailto:jklymak@coas.oregonstate.edu

http://pender.coas.oregonstate.edu/WorkTools.html